UNIVERSITY OF PITESTI
FACULTY OF MECHANICS AND TECHNOLOGY
SCIENTIFIC BULLETIN
AUTOMOTIVE series, year XVI, no.20 (1)

ON THE EFFECTS OF THE VALVE LIFTING HEIGHT UPON THE FILLING PROCESS[1]

Victor IORGA-SIMĂN[1], Adrian CLENCI[1], Pierre PODEVIN[2], Georges DESCOMBES[2]
[1]University of Pitesti, Romania
[2]Conservatoire National des Arts et Métiers, France

Abstract:

This investigation presents results from a 2D numerical simulation of the air flow within an engine presenting the possibility to continuously vary the intake valve lift during operation. Actually, for the case of still having the throttle plate, the purpose was to obtain results about air velocity, turbulence at the valve gap, for different openings of throttle plate and different valve lifts between 1 and 8.5 mm. Additionally, the throttle-less situation was investigated, too.

Thus, the paper's goal is to make a correlation between cylinder and manifold pressure drop and air velocity at the valve gap for the case of a certain opening of throttle plate and for different intake vale laws.

The most usual numerical method in Computational Fluid Dynamics (CFD) is finite volume. The CFD numerical simulations were made using the numerical code FLUENT choosing the k-ω SST turbulence model.

Keywords: CFD, valve lifting, flow field, 2D model

INTRODUCTION

As an energetic source, from the power density, stored energy and autonomy standpoint, the internal combustion engine still remains an actual solution, [1]. The increasing focus on the environmental impacts of hydrocarbon fuel based power generation has led to increased research efforts to reduce CO2 emissions, which mean improving the engine thermal efficiency.

During most of its average life, a road engine is run under low load and low speed conditions. It is known that load reduction in spark-ignition engines is traditionally realized by introducing additional losses during the intake stroke by means of a throttle valve. In these operating points, the engine efficiency decreases from the peak values (already not very high) to values dramatically lower.

The optimization of intake valve timing can provide significant reductions in pumping losses at part load operation, [3].

Our studies revealed that the ability to control valve lift certainly offers the ability to control intake air mass but also has the added benefit that it improves fuel-air mixing process and controls air motion. This is particularly important at idle and low part loads when low lifts are to be used for achieving the required power, [1].

Performing experiments on an engine is difficult because of the complexity of this mechanical system, especially when flow measurements are involved. Numerical experiments have the advantage that an expensive and time consuming measurement set-up is not necessary. Because of the increasing power of computers, the processes in an internal combustion engine can be modeled in more and more detail, [5]

The main goal of this paper is to perform a 2D CFD study on the effects of valve lifting height on the single cylinder filling process, using FLUENT software.

[1] *This article was produced under the project "Supporting young Ph.D students with frequency by providing doctoral fellowships", co-financed from the EUROPEAN SOCIAL FUND through the Sectoral Operational Program Development of Human Resources.*

CFD SIMULATION THEORY

The first step in Fluent was to import the mesh, to verify and scale it. Next, pressure values needed to be assigned to the inlet and outlet of 2D model. Implicit solver and k-ω SST turbulence model was used to simulate the air flow. The turbulent k-ω SST analysis typically took 1800-2000 iterations to converge.

k-ω SST model description

The shear-stress transport (SST) k-ω model was developed by Menter to effectively blend the robust and accurate formulation of the k-ω model in the near-wall region with the free-stream independence of the k-ω model in the far field, [2]

Transport Equations for the SST k-ω Model

k = turbulence kinetic energy,
ω = specific dissipation rate,

$$\frac{\partial}{\partial t}(\rho k)+\frac{\partial}{\partial x_i}(\rho k u_i)=\frac{\partial}{\partial x_i}\left(\Gamma_k \frac{\partial k}{\partial x_j}\right)+\widetilde{G}_k+Y_k+S_k \tag{1}$$

$$\frac{\partial}{\partial t}(\rho \omega)+\frac{\partial}{\partial x_i}(\rho \omega u_i)=\frac{\partial}{\partial x_i}\left(\Gamma_\omega \frac{\partial \omega}{\partial x_j}\right)+\widetilde{G}_\omega+Y_\omega+S_\omega \tag{2}$$

$\widetilde{G}_k$, represents the generation of turbulence kinetic energy, k

$$G_k=-\rho\overline{u_i' u_j'}\frac{\partial u_j}{\partial x_i} \tag{3}$$

G_ω, represents the generation of specific dissipation rate, ω

$$G_\omega=\alpha\frac{\omega}{k}G_k \tag{4}$$

Γ_k and Γ_ω represent the effective diffusivity of k and ω,

$$\Gamma_k=\mu+\frac{\mu_t}{\sigma_k} \tag{5}$$

and

$$\Gamma_\omega=\mu\frac{\mu_t}{\sigma_\omega}, \tag{6}$$

where σ_k and σ_ω are the turbulent Prandtl numbers for k and ω, respectively

$$\sigma_k=\frac{1}{F_1/\sigma_{k,1}+(1-F_1)/\sigma_{k,2}} \tag{7}$$

$$\sigma_\omega=\frac{1}{F_1/\sigma_{\omega,1}+(1-F_1)/\sigma_{\omega,2}} \tag{8}$$

The turbulent viscosity, μ_t, is computed as follows:

$$\mu_t=\frac{\rho k}{\omega}\frac{1}{\max\left[\frac{1}{\alpha^*},\frac{SF_2}{a_1\omega}\right]}, \tag{9}$$

where S is the strain rate magnitude,

α^* is defined as:

$$\alpha^* = \alpha_\infty^* \left(\frac{\alpha_0 + \mathrm{Re}_t / R_k}{1 + \mathrm{Re}_t / R_k} \right) \tag{10}$$

where: $\mathrm{Re}_t = \frac{\rho k}{\mu \omega}$, $R_k = 6$, $\alpha_0^* = \frac{\beta_i}{3}$, $\beta_i = 0.072$

The blending functions, F_1 and F_2, are given by:

$$F_1 = \tanh\left(\Phi_1^4\right), \tag{11}$$

$$\Phi_1 = \min\left[\max\left(\frac{\sqrt{k}}{0.09\omega y}, \frac{500\mu}{\rho y^2 \omega} \right), \frac{4\rho k}{\sigma_{\omega,2} D_\omega^+ y^2} \right], \tag{12}$$

$$D_\omega^+ = \max\left[2\rho \frac{1}{\sigma_{\omega,2}} \frac{1}{\omega} \frac{\partial k}{\partial x_j} \frac{\partial \omega}{\partial x_j}, 10^{-10} \right], \tag{13}$$

$$F_2 = \tanh\left(\Phi_2^2\right), \tag{14}$$

$$\Phi_2 = \max\left[2 \frac{\sqrt{k}}{0.09\omega y}, \frac{500\mu}{\rho y^2 \omega} \right], \tag{15}$$

where y is the distance to the next surface and D_ω^+ is the positive portion of the cross-diffusion term D_ω

$$D_\omega = 2\left(1 - F_1\right) \rho \sigma_{\omega,2} \frac{1}{\omega} \frac{\partial k}{\partial x_j} \frac{\partial \omega}{\partial x_j}. \tag{16}$$

The model constants are, [2]:

Table 1

$\sigma_{k,1}$	$\sigma_{k,2}$	$\sigma_{\omega,1}$	$\sigma_{\omega,2}$	$\beta_{i,1}$	$\beta_{i,2}$	a_1
1,176	1,0	2,0	1,168	0,075	0,0828	0,31

GEOMETRY AND MESH GENERATION

The geometry engine was created using the CATIA V5R19 software, and is represented in Figure 1.

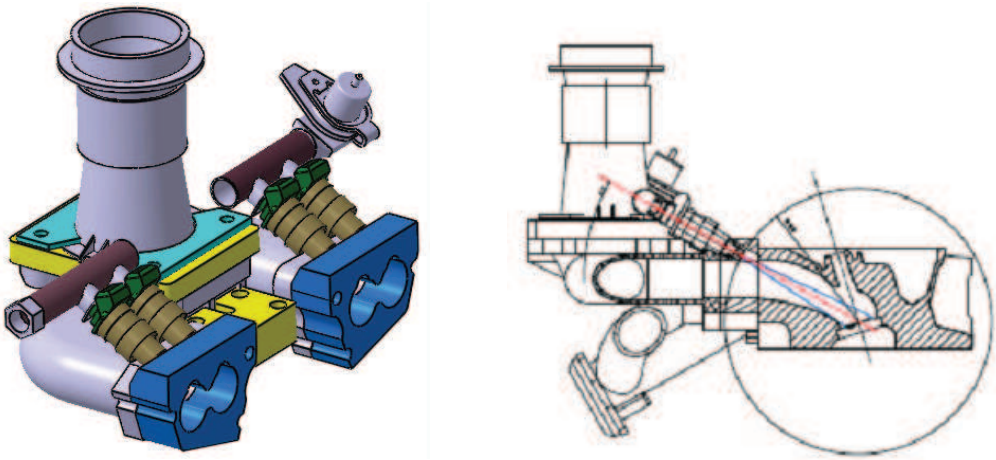

Figure 1. Geometry model

The main components of the 2D calculation model are shown in figure 2 and table 2.

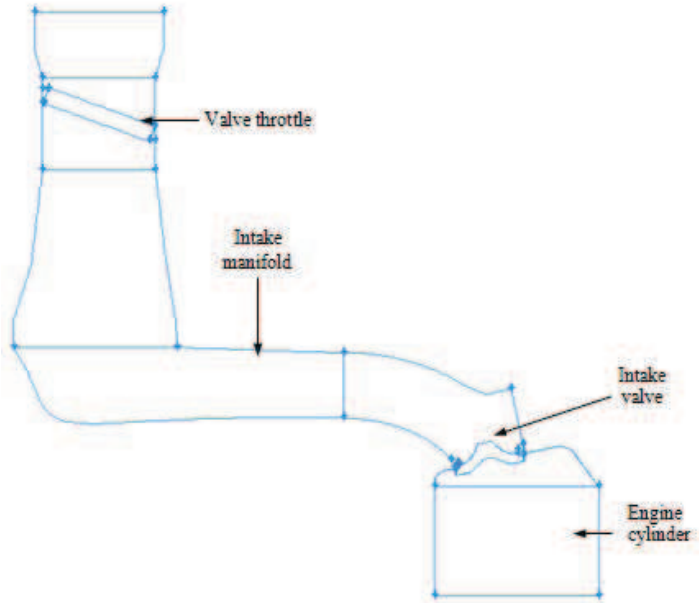

Figure 2. Components calculation model

Table 2. Basic dimensions of the model.

Throttle valve diameter [mm]	51.4
Intake manifold diameter [mm]	29.53
Intake valve diameter [mm]	31.6
Valve seat length [mm]	2.81
Cylinder diameter [mm]	75

Geometry was transformed in an IGES format. This **.igs* file format, used by several software packages to exchange geometries, is imported in the pre-processor Gambit, which is part of the CFD package Fluent. The IGES geometry file had to be processed in order to be able to mesh it.

The geometry grid is composed of 41935 cells. Quad cells have been used for the grid generation because it provides better accuracy and stability than triangular cells. For particular zones (between the throttle plate and its body) eight new surfaces have been made in order to obtain an adaptation to the geometry shape. Each zone has been meshed separately and contains a number of 1735 cells with dimensions ranging 0.1mm and 0.2mm with an interval count between 8-23 (figure 3).

The computational domain was divided in nine boundary conditions types and eleven continuum types for fluid. Pressure inlet is one boundary condition in the throttle plate body. The pressure outlet was chosen as boundary condition at the BDC (bottom dead center) in cylinder.

In this simulation, air is assumed as ideal gas. With this assumption, the density will be variable but other properties like viscosity and thermal conductivity will be permanent (table 2)

Table 3 Air input properties

Atmospheric pressure *[Pa]*	101325
Temperature *[K]*	300
Specific heat at constant pressure $[J/kg \cdot K]$	1006.43
Thermal conductivity $[W/m \cdot °C]$	0.0242
Dynamic viscosity $[kg/m \cdot s]$	$1.7894 \cdot 10^{-5}$

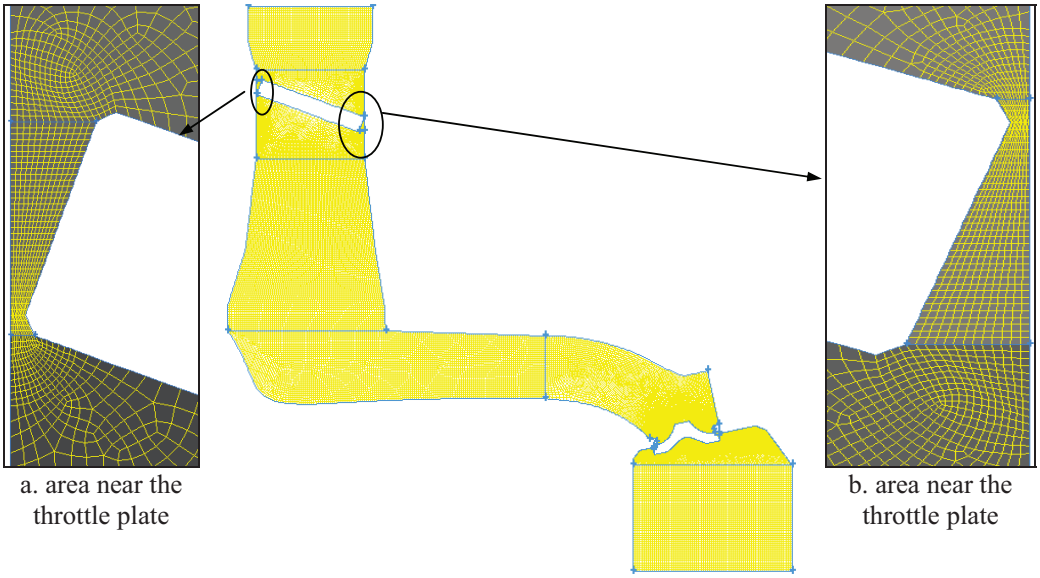

a. area near the throttle plate

b. area near the throttle plate

Figure 3. Surface mesh adaptation

The study was performed to simulate the stationary airflow at an engine speed of 800 rev/min, corresponding to the idle operation. In order to set the boundary conditions, data were taken from experiments performed in a steady-state flow within the variable intake valve lift engine fitted with in-cylinder and intake manifold pressure sensors. Figure 4 presents a general view of the engine test bench.

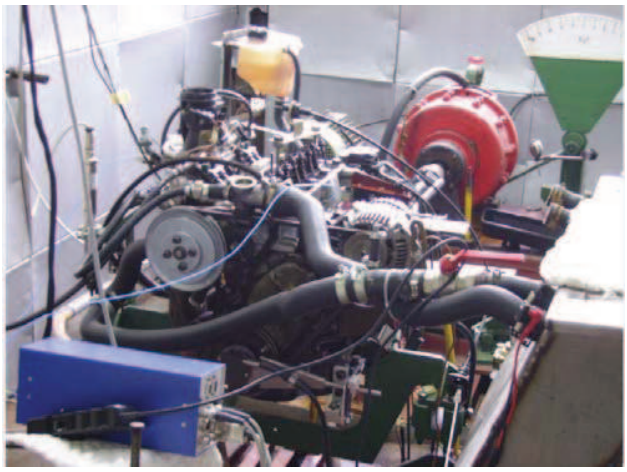

a. engine test bench: general view

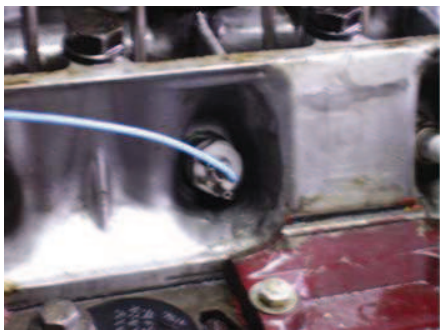

b. piezoelectric pressure traducer

c. angular encoder. TDC transducer

Figure 4. The architecture of engine test bench

For the unfired situation, the in-cylinder pressure variations, corresponding to different throttle plate openings (table 4) and intake valve lifts, were drawn using AVL IndiModul.

Table 4. Angular opening valve throttle

$\varphi_{throttle}$ [°]										
18	20	21.6	23.6	25.2	26.8	28.8	30.8	31.6	35	90

For instance, in figure 5 *a and b* are exposed the instantaneous variation of in-cylinder pressure and manifold pressure for 1.365 mm and 1.864 mm intake valve lifts (H_{SA}), for each of the throttle plate openings, listed in table 4.

Pressure waves are due to timing of the intake valve in each of the four cylinder engine. Minimum and maximum peaks of cylinder pressure were recorded for the minimum throttle plate opening at φ =18° (see the red curve in figure 5), respectively maximum throttle opening φ = 90° (see the blue curve in figure 5).

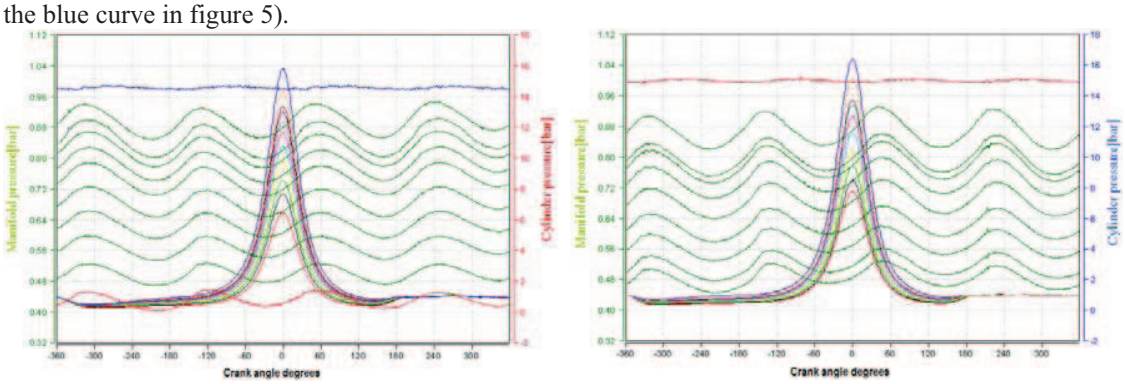

a. H_{SA} *= 1.365 mm* *b.* H_{SA} *= 1.864 mm*

Figure 5. The variation of pressure in cylinder and intake manifold

The in-cylinder pressure values measured during the intake stroke (figure 6) have been mediated. As stated before, the mean in-cylinder pressure value is used as a boundary condition for numerical simulation.

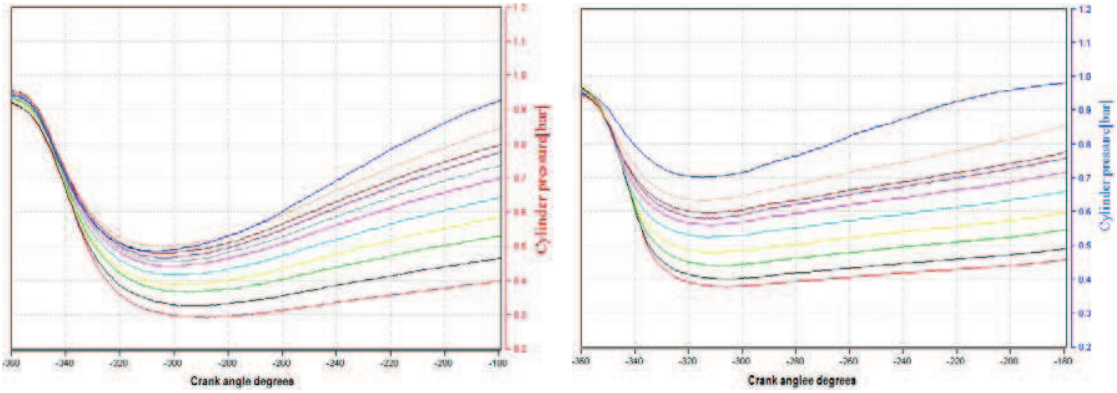

a. H_{SA} *= 1.365 mm* *b.* H_{SA} *= 1.864 mm*

NB. The red curve corresponds to the minimum throttle opening and the blue one for the maximum opening (see table 3)

Figure 6. Variation of pressure in cylinder during intake stroke

RESULTS AND DISCUSSION

As far as the validation of the CFD calculation is concerned, the following reasoning was used: the pressure in the intake manifold, obtained through direct measurement, will be compared with the pressure calculated by numerical simulation.

The numerical simulation considered two cases:

1. for a fixed opening of the throttle plate (φ=25.2°), several laws of intake valve movement were explored (see table 5),
2. the throttle-less situation, under the same movement laws for the intake valve.

For the first case examined, corresponding to a throttle opening at 25.2°, measured or calculated data are presented in Table 5

Table 5. Throttle valve open φ = 25.2°

H_{sa} [mm]	A_{sa} [mm^2]	p_{cyl} [mbar]	p_{col} [mbar] *(measured)*	p_{col_CFD} [mbar] *CFD*	Δp_{cyl_col} [mbar]	W_{sa} [m/s]	Δp_{col_atm} [mbar]	W_{obt} [m/s]
1.365	94.7	552	680	652	128	183.5	361	287
1.864	130	565	628	607.6	63	143	405.4	308
2.05	142.2	569	610	609	41	122	404	306
3.075	213	570	610	584.1	40	94	428.9	319
8.47	587.84	613	678	613.6	65	42	399.4	304

By analyzing the graph below, one may notice that the two curves describing the measured manifold pressure (the blue curve), and, respectively, the pressure calculated by CFD Fluent, have similar shapes, though they are different in point of absolute value. In other words, the real physical phenomenon is reproduced through simulation. The same graph serves to evince the gap between the value of the measured manifold pressure value, and the calculated value. Its span ranges between the following limits: 0.16% for H=2.05 mm, and 9.5% for H=8,47 mm.

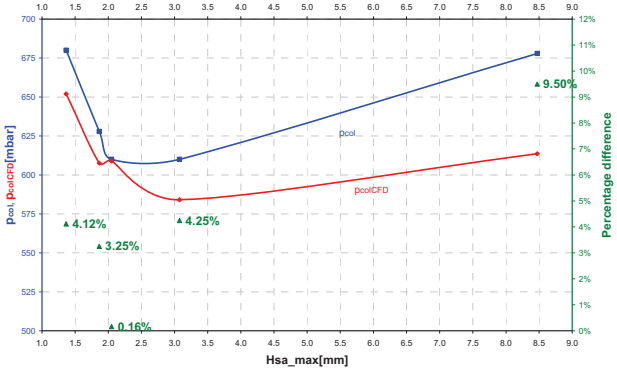

Figure 7. Comparison between manifold pressure values measured and calculated using Fluent CFD

In Figure 8 a continuous increase in the absolute in-cylinder pressure can be noticed, once with an increase in the maximal height to which the intake valve is lift, which signifies a reduction in the pumping losses. As far as the absolute pressure in the intake collector is concerned, it initially has, as can be noticed, a downward evolution, accountable for by the fact that an increase in the flowing cross-section allows to transfer the depression (vacuum) from the cylinder into the manifold. The rising evolution, which follows can be explained through the fact that, with the increase in the maximal lifting height, the intake valves open sooner on the cycle. Actually, in figure 9 one can notice that, for the reduced movement laws of the intake valves, it is by no means the case of an anticipated opening, quite on the contrary, it is a delay with respect to the TDC.

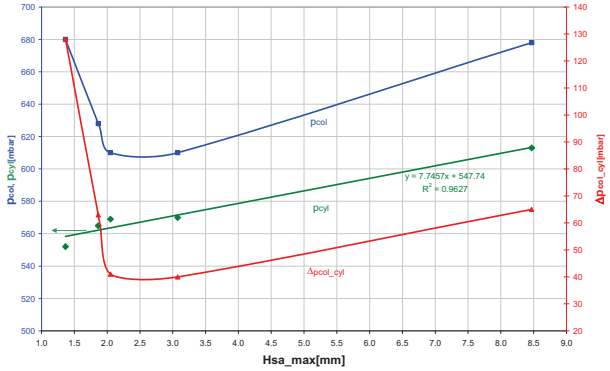

Figure 8. Evolution of $\Delta_{pcol\text{-}cyl}$ for different maximum valve lift

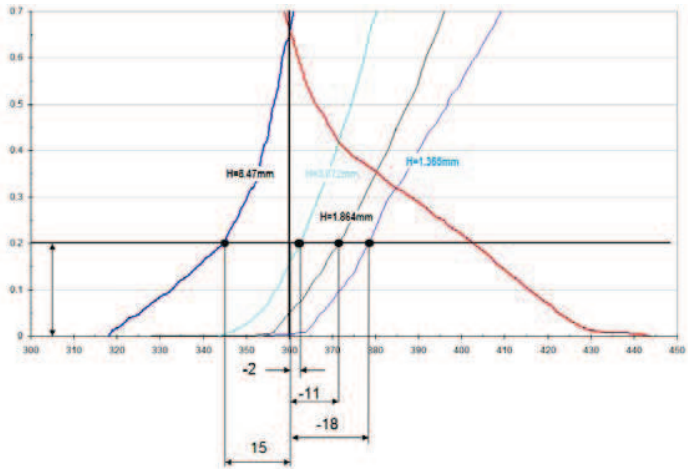

Figure 9. The intake valve laws.

The difference in pressure between the intake manifold and the in-cylinder determines the flow velocity W_{sa} of the fluid through the port of the intake valve, as shown in Figure 10. The flow velocity W_{sa} is also influenced by the instantaneous area provided by the intake valve's opening A_{sa}.

The curves obtained in Figure 10 highlight the following:

- along the first segment of the graph, the flow velocity W_{sa} decreases, once with the decrease in the value Δp_{col_cyl} and the increase in the instantaneous area A_{sa};

- for the height of valve raising H = 3.07 mm, corresponding to an instantaneous area $A_{sa} = 213$ mm^2, the difference in pressure Δp_{col_cyl} increases. That increase in the value of Δp_{col_cyl} does not determine, however, a corresponding increase in the speed of the flow under the valve. The explanation of the fact consists in the fact that, under the said circumstance, the overwhelming effect is represented by the increase in the passing instantaneous area A_{sa}.

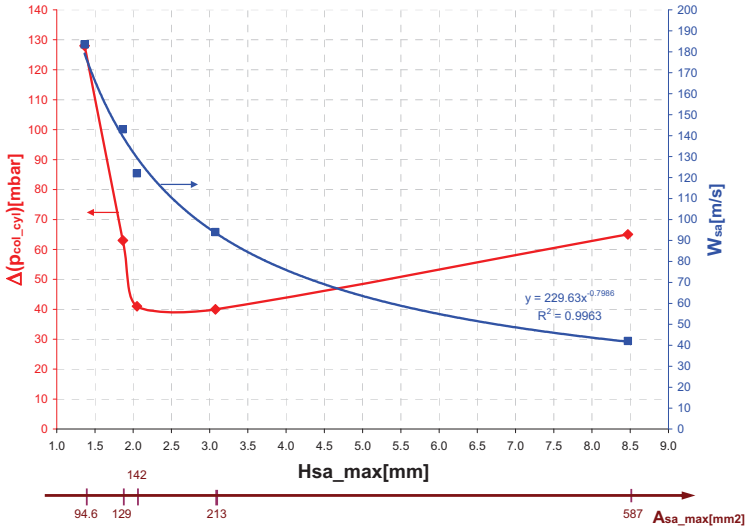

Figure 10. The flow velocity under valve

Using values obtained by CFD simulation, in figure 11 is displayed graphically, on the one hand, the difference pressure between the intake manifold and the atmosphere, according to the law of motion imposed at the inlet valve, and, on the other hand, the flow velocity.

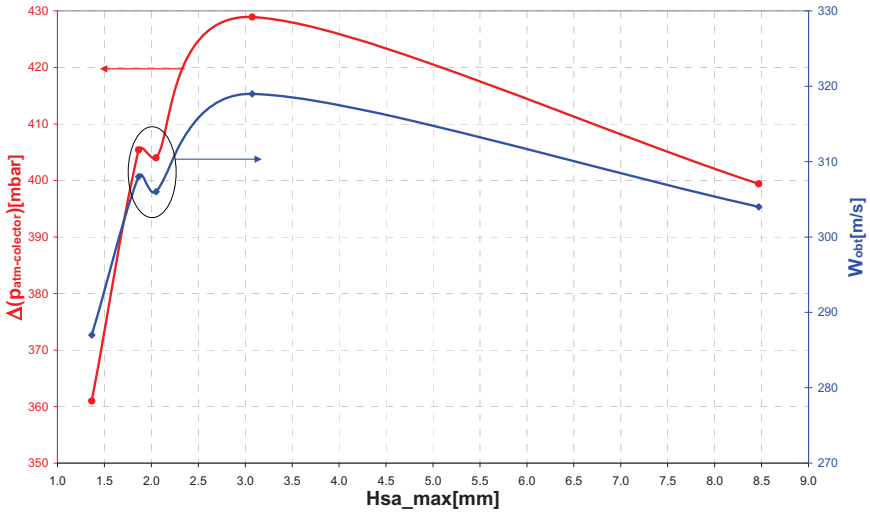

Figure 11. The flow velocity under throttle valve

What should be noted in this figure is that the numerical calculation results confirm the hypothesis that for a section of passage remained constant, the flow velocity established in that area is caused by the difference pressure.

The values shown above, the speed under the intake valve as those under the throttle valve, have been obtained from numerical simulations using Fluent software. Figure 12 presents the speed distribution under intake valve and throttle plate for two of the simulated cases: minimum and maximum intake valve lifts.

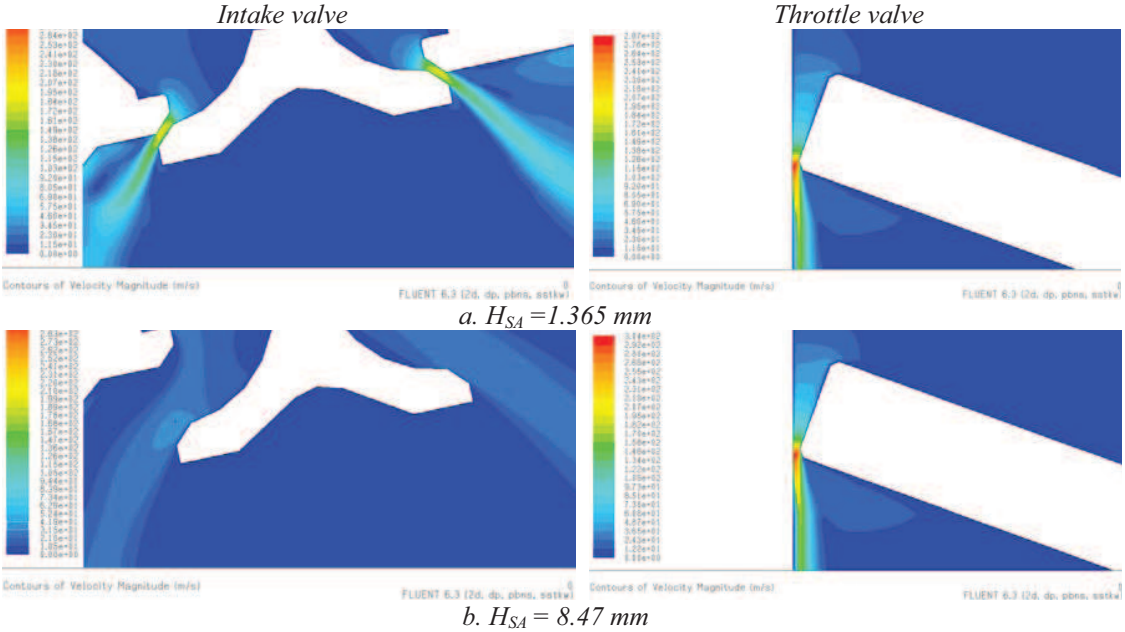

a. H_{SA} =1.365 mm

b. H_{SA} = 8.47 mm

Figure. 12 The fields of speeds under the intake valve and throttle

The second situation analyzed is that of the geometrically model without throttle plate – throttle-less (figure 15).

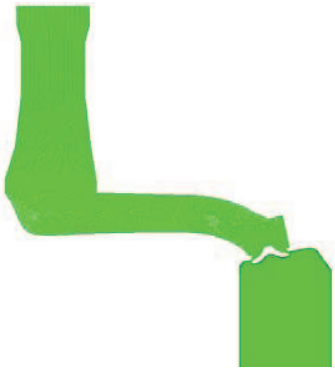

Figure 14. Geometry of calculation model without valve throttle

Measured or calculated values obtained for throttle-less 2D model are shown in the following table:

Table 6

H_{sa} [mm]	A_{sa} [mm2]	P_{cyl} [mbar]	P_{col} [mbar] *(measured)*	p_{col} [mbar] *CFD*	$\Delta p_{cyl\ col}$ [mbar]	W_{sa} [m/s]
1.365	94.7	679	980	979	301	296
1.864	130	837	995	994.8	158	217
2.05	142.2	847	980	979	133	201
3.075	213	912	991	990	79	186
8.47	587.84	968	991	989.3	23	123

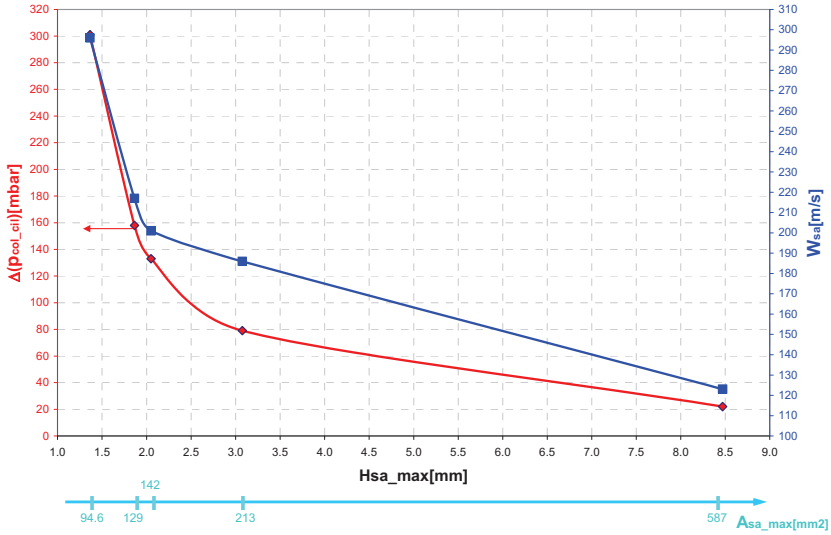

Figure 15. Velocity flow under valve

The chart above illustrates the flow velocity under the intake valve provided for different heights of the valve lift and without throttle valve. It is noted that with decreasing pressure drop between the manifold and cylinder the speed W_{SA} decreases.

Velocity and pressure contours obtained by numerical simulation calculations for the throttle-less intake system are shown in the figure below:

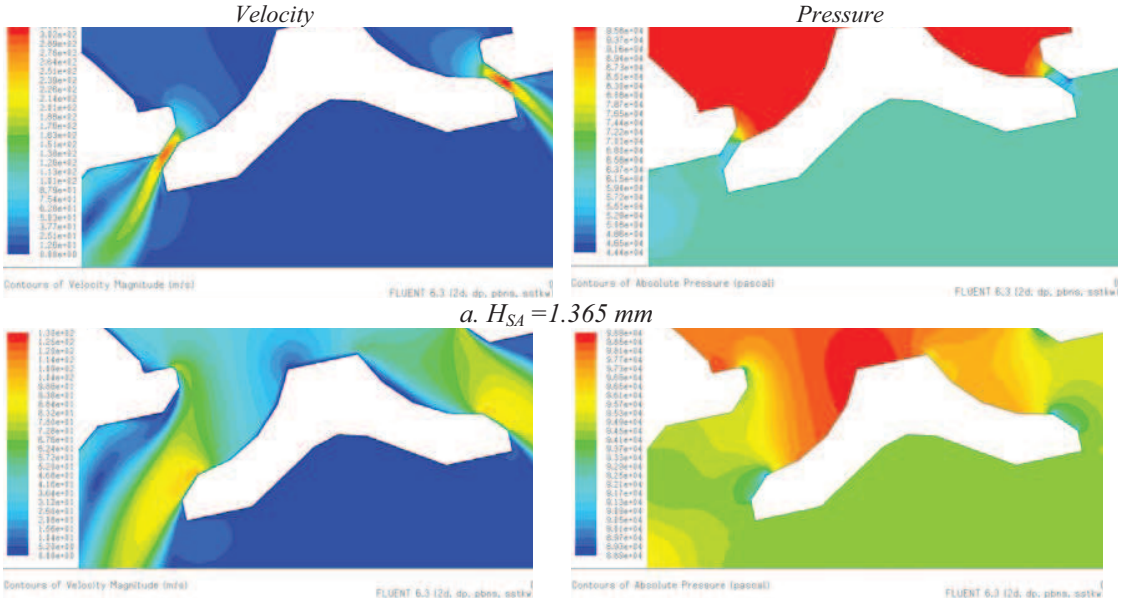

a. H_{SA} *=1.365 mm*

b. H_{SA} *= 8.47 mm*

Figure 16. Velocity and pressure field near intake valve

CONCLUSIONS AND FUTURE WORKS

The reduction of fuel consumption is a fundamental aspect of the automotive industry. This comes from customers, as well as from legal demands. While diesel engine made enormous progress during the last period and features good fuel economy, the spark ignition engine still suffers from this point of view. Variable valve actuation offers many opportunities to improve the spark ignition engine's performances in areas like fuel economy, emissions and power density and it seems it will become the next industry standard on gasoline engines.

This study's goal was to obtain some insights about what's happening during the intake stroke of a variable intake valve lift prototype engine. Therefore, the study was performed to simulate the airflow at an engine speed of 800 rpm, corresponding to the idle operation. Actually, for the case of still having the throttle plate, the purpose was to obtain results about air velocity at the valve gap, for different openings of throttle plate and different valve lifts between 1 and 8.5 mm. Thus, the purpose was to make a correlation between cylinder and manifold *pressure drop* and air velocity at the valve gap for the case of different openings of throttle plate or for the throttle-less situation and for different intake vale laws. Small intake valve lifts are particularly important at low part loads and speeds due to the fact that they improve fuel-air mixing process and controls air motion, which – apparently – has the main weight in the equation of fuel consumption reduction.

Certainly, the 2D modeling and simulation has some limitations, therefore for the future, the model will get the other dimension and, equally, unstationary numerical simulation will be performed by taking into consideration the intake valve and piston motions.

REFERENCES

[1] Clenci A., Podevin P., Descombes G., Berquez J. - *Variable intake valve lift on spark ignition engine and its effects on idle operation*, EAEC Congress, Bratislava 2009

[2] Fluent 6.2 „*User's guide*. Fluent Inc.

[3] G. Fontana, E. Galloni - *Variable valve timing for fuel economy improvement in a small spark-ignition engine*, Applied Energy 86 (2009) 96–105

[4] M.H. Shojaeefard, A.R., Noorpoor - *Flow Simulation in Engine Cylinder with Spring Mesh*, American Journal of Applied Sciences 5 (10): 1336-1343, 2008

[5] Smits, J.J.M - *Modeling of a fluid flow in an internal combustion engine*, 2006